Journal of Power Sources 376 (2018) 161–167

Contents lists available at ScienceDirect

Journal of Power Sources

journal homepage: www.elsevier.com/locate/jpowsour

# Enhanced Fe dispersion via "pinning" effect of thiocyanate ion on ferric ion in Fe-N-S-doped catalyst as an excellent oxygen reduction reaction electrode

Chengyong Shu[a], Yuanzhen Chen[a,*], Xiao-Dong Yang[b], Yan Liu[a], Shaokun Chong[a], Yuan Fang[c], Yongning Liu[a], Wei-Hua Yang[b]

[a] State Key Laboratory for Mechanical Behavior of Materials, School of Material Science and Engineering, Xi'an Jiaotong University, Xi'an 710049, PR China
[b] College of Materials Science and Engineering, Huaqiao University, Xiamen, Fujian 361021, PR China
[c] School of Materials Science and Engineering, Shaanxi University of Science and Technology, Xi'an 710021, PR China

## HIGHLIGHTS

- Improved iron salts stability and dispersibility by the introduction of $SCN^-$.
- High oxygen reduction reaction activity in both acidic and alkaline medium.
- Operation for 400 h as a cathode electrode in direct methanol fuel cell.
- Have an explicit cyanide N and pyrrolic N functional groups.

## GRAPHICAL ABSTRACT

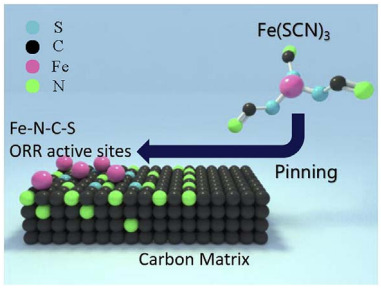


## ARTICLE INFO

*Keywords:*
$H_2/O_2$fuel cells
Acid medium
Direct methanol fuel cell
Oxygen reduction reaction

## ABSTRACT

In this study, by using thiocyanate as an iron ion dispersing agent, the pinning effect of thiocyanate ion ($SCN^-$) enables the high dispersion of $Fe^{3+}$ in a nitrogen-doped carbon polymer and significantly promotes ORR catalysis in both acidic and alkaline media. It shows 47.3 A $g^{-1}$ kinetic ORR current density in 0.1 M $H_2SO_4$ solution at 0.8 V vs. RHE. In addition, $SCN^-$ can dope into the base material and modify the surface of catalysts, which generates strong cyanide N functional groups. Additionally, it also has a higher BET surface area and more uniform granularity, which accounts for the enhancement in mass transport.

## 1. Introduction

Electrocatalysts used for the oxygen reduction reaction (ORR) are key for the development of renewable energy technologies since slow ORR on the cathode limits the energy conversion efficiency of fuel cells and a substantial cathode catalyst is required to meet the actual power demand [1]. The $H_2/O_2$ fuel cell vehicle is a good example. Although Pt and its alloys are currently the most efficient catalysts, the substantial use of these expensive catalysts have resulted in high cost PEMFC, which account for half of the cost of the fuel cell stack [2]. Moreover, a Pt catalyst often suffers from decreasing activity due to poisoning by CO and NO and a low tolerance to methanol [3], which prevent the large scale application of Pt catalysts.

Heteroatom-doped carbon materials are metal-free electrocatalysts, and they have been extensively researched to replace commercial Pt/C catalysts in the ORR and OER [4–8]. For decades, significant progress has been achieved in preparing and understanding ORR catalysts in PEMFC [9,10]. Dai [11,12] and other researchers [13,14] reported highly active ORR catalysts such as nitrogen-doped carbon nanotubes, non-precious metal catalysts or metal-free catalysts (including the

* Corresponding author.
*E-mail address:* cyz1984@xjtu.edu.cn (Y. Chen).

https://doi.org/10.1016/j.jpowsour.2017.11.093
Received 7 October 2017; Received in revised form 21 November 2017; Accepted 28 November 2017

doping of nitrogen, boron or phosphor atoms), and since then, those materials have played an important role in the rapid development of ORR electrocatalysts in recent years. Many documents further indicate that dual-doping or tri-doping heteroatoms, along with the use of a transition metal applied to carbon materials, can develop various synergistically enhanced ORR catalysts for fuel cell applications [7,15–17].

There is general agreement that Fe plays an important role in enhancing the ORR activity of the catalysts [18–20]. It was confirmed that upon ball-milling, pyrolysis in an $NH_3$ or $N_2$ atmosphere and other critical steps, Fe-$N_x$/C catalysts display a considerable ORR activity [21]. Previous works showed a positive correlation between the Fe/N content and ORR activity, revealing the advantages of replacing Pt-based ORR catalysts. However, the complex N-C structure that appears after pyrolysis still does not provide any further understanding of the active sites of the non-precious metal cathode catalyst [22,23], and it is hard to develop an Fe-N-C catalyst with high-density active sites [24,25]. Additionally, in practical PEMFC applications, these non-precious metal or metal-free catalysts must tolerate strong acidic and corrosive environments [26] and the poor mass transfer ability due to the increased thickness of the catalyst layer in a high loading situation, which is caused by the poor ORR activity [27]. Therefore, it is necessary to enhance the catalytic ability of the catalysts, the efficiency of the mass transfer, and the stability of the catalysts.

Herein, we propose a strategy of designing highly microporous Fe/N/S tri-doped electrocatalyst materials for ORR, of which the most important point is the addition of thiocyanate. As shown in Fig. 1, first p-Phenylenediamine (pBDA) was combined with carbon black by a polymerization process, and it served as the source of N and C; then, the mixture of $SCN^-$ and $Fe^{3+}$-containing salts were deposited onto the surface of the polymer through a rotary evaporation process. Finally, the Fe/N/S-doped microporous carbon material was prepared by pyrolysis of the precursor in Ar atmosphere. The $SCN^-$ could maintain their structure and retain a suitable binding force with $Fe^{3+}$, preventing the Fe ions from being oxidized to a stable phase (e.g., $Fe_2O_3$, FeO) in the early heat treatment step and, meanwhile, reducing the occurrence of particle agglomeration. Through the bonding between carbon and nitrogen atoms, the atoms in $SCN^-$ were successfully doped into the surface of the matrix material to modify the surface property, which was accompanied by the formation of a more microporous surface with a higher specific surface area. In addition, an explicit pyridinic N and cyanide N functional group structure domain was formed. The Fe atoms, which were pinned with $SCN^-$, were naturally dispersed around these N-C functional groups, and they probably transformed into Fe-N-C active sites during the post high-temperature heat treatment. Therefore, the as-prepared Fe-N-S tri-doped electrocatalyst achieved a higher ORR performance and showed a very high and stable power output in DMFCs and $H_2/O_2$ cells.

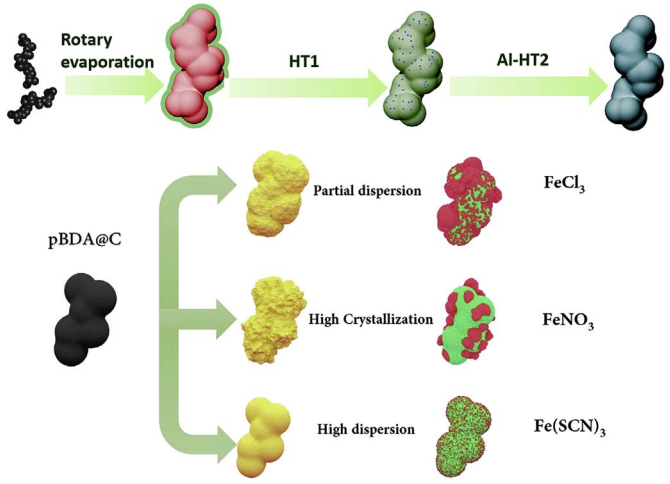


**Fig. 1.** A schematic representation of the process of material preparation.

## 2. Results and discussion

The morphologies of three catalysts with the addition of different kinds of Fe salts in different steps were observed. Figure S.1 shows the change in the carbon particles before and after the N-source coating; the particle size was increased from approximately 50 nm to approximately 100 nm. In the rotary evaporation process (Fig. 2.a, f, k), we found that the Fe salts were mostly coated on the surface of pBDA@C, but it was clear that the coating layers in Fe-pBDA@C-Cl and Fe-pBDA@C-$NO_3$ showed large bulk aggregates, while the Fe-pBDA@C-SCN was evenly coated. Derived from the XRD information (Fig. 2.p), the coating layer of Fe-pBDA@C-Cl consisted of the mixture of a substantial amount of iron chloride hydrate crystals and iron oxide crystals. While the coating layer of Fe-pBDA@C-$NO_3$ was mainly an iron oxide hydroxide. It was noticeable that the XRD spectrum of Fe-pBDA@C-SCN only displayed the feature peaks of ammonium chloride but no peak of the iron salt, which could be attributed to the displacement reaction between $FeCl_3$ and $NH_4SCN$ [28]. Ammonium chloride first precipitated and coated the surface of the pBDA@C particles, and meanwhile, the force from the $SCN^-$ hindered the ability of the iron ions to crystallize. Thus, there was no obvious peak of Fe in the XRD results in the Fe-pBDA@SCN samples after the evaporation process.

After the 1st heat treatment (HT1), the type of iron salts and their crystal morphology in the surface of Fe-pBDA@C-$NO_3$ had changed significantly. In Fig. 2.g, it could be clearly observed that large bulk crystals were formed. The XRD spectrum confirmed that the main iron crystal was $Fe_3O_4$ for Fe-pBDA@C-$NO_3$ (Fig. 2 q). There were also iron crystals distributed around the Fe-pBDA@C-SCN and Fe-pBDA@C-Cl, for which the main crystals were FeS and $Fe_3C$, respectively, but they were not particularly obvious in the SEM (Fig. 2.b, l). TEM images are shown in Fig. 2. c, m. The bulk crystal and fine crystals in each sample are obvious. Different kinds of anions of iron salts directly affect the morphology and dispersion of the iron crystals produced in the pyrolysis steps. Due to the "pinning" effect of the $SCN^-$, the iron salts do not tend to form large chunks of crystals, but rather many fine crystals, which are scattered around the carbon substrate. In an attempt to create more active sites, all samples were leached by acid, and their morphologies were observed, as shown in Fig. 2.d, i, n. Compared with the materials after the first heat treatment, most of these Fe solids were removed after the acid leaching process, and there were only broad carbon peaks in the XRD spectrum (Fig. 2.r). Even though there is no obvious sign of Fe, the mapping spectra of the above samples after the acid leaching process obviously display the homogeneous distribution of Fe on the surface of the carbon matrix (figure S.2).

Thermogravimetric analysis (TGA) at a heating rate of 10 K $min^{-1}$ in $N_2$ atmosphere was used to test the stability of the N-containing precursors adding iron salts with different anions. As shown in figure S.3 a, the first weight loss of pBDA@C started at 50 °C, which represents the evaporation of water and other organic molecules. The decomposition started at 207.9 °C and showed rapid weight loss (30% weight loss) process until 400 °C. During the whole heat process to 1000 °C, the total weight loss was 41%. The weight loss curves have a great change when other different anions salts were added into it. For Fe-pBDA@C-Cl (figure S.3 b), in addition to the decomposition of pBDA@C, there were two other weight loss processes; the first occurred at a range from 120 to 210 °C, which indicated the removal of $H_2O$ and HCl from iron chloride hydrate, and the second occurred at a range from 320 to 500 °C, which related to the decomposition of anhydrous ferric chloride with HCl(g) and $Cl_2$(g) [12,29,30]. For the plot of Fe-pBDA@C-$NO_3$ (figure S.3 c), obviously, the rapid weight loss process occurs earlier, and shows a main endothermic weight loss process at 125 °C, which represents the transformation of iron oxide hydroxide to iron oxide [30]. For Fe-pBDA@SCN (figure S.3.d), a similar weight loss